AFRL-RX-WP-JA-2016-0216

ELECTRONIC AND OPTICAL PROPERTIES OF TITANIUM NITRIDE BULK AND SURFACES FROM FIRST PRINCIPLES CALULATIONS (POSTPRINT)

Faisal Mehmood, Ruth Pachter, Neil R. Murphy, and Walter E. Johnson

AFRL/RX

Faisal Mehmood

General Dynamics Information Technology

19 MARCH 2015
Interim Report

(STINFO COPY)

AIR FORCE RESEARCH LABORATORY
MATERIALS AND MANUFACTURING DIRECTORATE
WRIGHT-PATTERSON AIR FORCE BASE, OH 45433-7750
AIR FORCE MATERIEL COMMAND
UNITED STATES AIR FORCE

REPORT DOCUMENTATION PAGE

Form Approved
OMB No. 0704-0188

1. REPORT DATE *(DD-MM-YY)*	2. REPORT TYPE	3. DATES COVERED *(From - To)*
19 March 2015	Interim	11 January 2013 – 19 February 2015

4. TITLE AND SUBTITLE
ELECTRONIC AND OPTICAL PROPERTIES OF TITANIUM NITRIDE BULK AND SURFACES FROM FIRST PRINCIPLES CALULATIONS (POSTPRINT)

5a. CONTRACT NUMBER
FA8650-09-D-5430-0025

5b. GRANT NUMBER

5c. PROGRAM ELEMENT NUMBER
61102F

6. AUTHOR(S)
1) Faisal Mehmood, Ruth Pachter, Neil R. Murphy, and Walter E. Johnson - AFRL/RX
2) Faisal Mehmood - GDIT

5d. PROJECT NUMBER
3002

5e. TASK NUMBER 0025

5f. WORK UNIT NUMBER
X0KU

7. PERFORMING ORGANIZATION NAME(S) AND ADDRESS(ES)
1) AFRL/RX
Wright Patterson AFB
Dayton, OH 45433
2) GDIT
5100 Springfield St. Suite 509
Beavercreek, OH 45431

8. PERFORMING ORGANIZATION REPORT NUMBER

9. SPONSORING/MONITORING AGENCY NAME(S) AND ADDRESS(ES)
Air Force Research Laboratory
Materials and Manufacturing Directorate
Wright-Patterson Air Force Base, OH 45433-7750
Air Force Materiel Command
United States Air Force

10. SPONSORING/MONITORING AGENCY ACRONYM(S)
AFRL/RXAP

11. SPONSORING/MONITORING AGENCY REPORT NUMBER(S)
AFRL-RX-WP-JA-2016-0216

12. DISTRIBUTION/AVAILABILITY STATEMENT
Distribution Statement A. Approved for public release: distribution unlimited.

13. SUPPLEMENTARY NOTES
PA Case Number: 88ABW-2015-1249; Clearance Date: 19 Mar 2015. This document contains color. Journal article published in the Journal of Applied Physics, Vol. 118, No. 19, November 2015. © 2015 AIP LLC. The U.S. Government is joint author of the work and has the right to use, modify, reproduce, release, perform, display, or disclose the work.
The final publication is available at http://dx.doi.org/10.1063/1.4935813

14. ABSTRACT *(Maximum 200 words)*
Prediction of the frequency-dependent dielectric function of thin films poses computational challenges, and at the same time experimental characterization by spectroscopic ellipsometry remains difficult to interpret because of changes in stoichiometry and surface morphology, temperature, thickness of the film, or substrate. In this work, we report calculations for titanium nitride (TiN), a promising material for plasmonic applications because of less loss and other practical advantages compared to noble metals. We investigated structural, electronic, and optical properties of stoichiometric bulk TiN, as well as of the TiN(100), TiN(110), and TiN(111) outermost surfaces. Density functional theory (DFT) and many-body GW methods (Green's (G) function-based approximation with screened Coulomb interaction (W)) were used, ranging from G0W0, GW0 to partially self-consistent sc-GW0, as well as the GW-BSE (Bethe-Salpeter equation) and time-dependent DFT (TDDFT) methods for prediction of the optical properties. Structural parameters and the band structure for bulk TiN were shown to be consistent with previous work. Calculated dielectric functions, plasma frequencies, reflectivity, and the electron energy loss spectrum demonstrated consistency with experiment at the GW0-BSE level.

15. SUBJECT TERMS
Dielectric function, spectroscopic ellipsometry, stoichiometry, surface morphology, titanium nitride (TiN), plasmonic,

16. SECURITY CLASSIFICATION OF:			17. LIMITATION OF ABSTRACT:	18. NUMBER OF PAGES	19a. NAME OF RESPONSIBLE PERSON (Monitor)
a. REPORT	b. ABSTRACT	c. THIS PAGE			Ruth Pachter
Unclassified	Unclassified	Unclassified	SAR	13	19b. TELEPHONE NUMBER *(Include Area Code)* (937) 255-9689

Electronic and optical properties of titanium nitride bulk and surfaces from first principles calculations

Faisal Mehmood,[1,2] Ruth Pachter,[1,a)] Neil R. Murphy,[1] and Walter E. Johnson[1]
[1]*Air Force Research Laboratory, Materials and Manufacturing Directorate, Wright-Patterson Air Force Base, Ohio 45433, USA*
[2]*General Dynamics Information Technology, Inc., Dayton, Ohio 45433, USA*

(Received 15 August 2015; accepted 2 November 2015; published online 18 November 2015)

Prediction of the frequency-dependent dielectric function of thin films poses computational challenges, and at the same time experimental characterization by spectroscopic ellipsometry remains difficult to interpret because of changes in stoichiometry and surface morphology, temperature, thickness of the film, or substrate. In this work, we report calculations for titanium nitride (TiN), a promising material for plasmonic applications because of less loss and other practical advantages compared to noble metals. We investigated structural, electronic, and optical properties of stoichiometric bulk TiN, as well as of the TiN(100), TiN(110), and TiN(111) outermost surfaces. Density functional theory (DFT) and many-body GW methods (Green's (G) function-based approximation with screened Coulomb interaction (W)) were used, ranging from G_0W_0, GW_0 to partially self-consistent sc-GW_0, as well as the GW-BSE (Bethe-Salpeter equation) and time-dependent DFT (TDDFT) methods for prediction of the optical properties. Structural parameters and the band structure for bulk TiN were shown to be consistent with previous work. Calculated dielectric functions, plasma frequencies, reflectivity, and the electron energy loss spectrum demonstrated consistency with experiment at the GW_0-BSE level. Deviations from experimental data are expected due to varying experimental conditions. Comparison of our results to spectroscopic ellipsometry data for realistic nanostructures has shown that although TDDFT may provide a computationally feasible level of theory in evaluation of the dielectric function, application is subject to validation with GW-BSE calculations. © *2015 AIP Publishing LLC*. [http://dx.doi.org/10.1063/1.4935813]

I. INTRODUCTION

Titanium nitride gained much interest in the last decades because of unique properties,[1–3] such as high hardness, high wear and corrosion resistance, which are useful for protective and decorative coatings,[4,5] compatibility with complementary metal-oxide-semiconductor (CMOS) processes, e.g., used as diffusion barriers and gate material,[6] or for solar cell application.[7] Recently, TiN thin films were suggested as alternative plasmonic materials,[8–12] exhibiting less loss and providing other practical advantages compared to noble metals. For example, comparing TiN and gold disk-shaped nanoparticles, it was shown that the TiN nanodisks are efficient local heat sources and outperform gold in the biological transparency window.[11] Furthermore, fabrication of epitaxial superlattices with thin film TiN as a plasmonic component for optical hyperbolic metamaterials demonstrated a higher photonic density of states than the gold- or silver-based respective nanomaterial structures.[12] In order to assess the bounds of performance of such materials, knowledge of the material properties is required in solving Maxwell's equations, e.g., with the finite-difference time-domain method.[13] In this case, a best fit of an experimental frequency-dependent dielectric function to an analytic expression is used in the simulated spectral region.

The frequency-dependent dielectric function of TiN thin films was characterized by spectroscopic ellipsometry (SE) in previous work,[8,14–21] analyzed, for example, with a Drude-Lorentz model $\varepsilon = \varepsilon_\infty - \frac{\omega_{pu}^2}{\omega_2 - i\Gamma_D\omega} + \sum_{j=1}^{l} \frac{f_j\omega_{0j}^2}{\omega_{0j}^2 - \omega^2 - i\Gamma_j\omega}$; ε_∞ is a background constant due to interband transitions, larger than unity due to higher-energy transitions not represented by the l Lorentz oscillators considered. In the Drude term, ω_{pu} is the unscreened plasma frequency, correlated with the free electron density and the metallic character, and Γ_D is a damping factor due to the scattering of electrons, determined by the inverse of the mean time between collisions, i.e., free electron relaxation time. The j Lorentz oscillators have interband excitation ω_{0j}, oscillator strength f_j, and damping factors Γ_j. Various parameters were varied to fit the SE data for TiN, e.g., the number of Lorentz oscillators,[22] where models with two or four Lorentz oscillators[16] were adopted.[14] Indeed, parameters that change the response of the film are generally not well defined, such as effects of deposition conditions, including stoichiometry, surface morphology and crystallinity, temperature, bias voltage, or substrate and thickness. For instance, the unscreened plasma frequency was shown to decrease substantially depending on the deposition temperature or nitrogen flow rates, while effects of substrate could be important for films thinner than 60 nm.[14] Below 5 nm, the dielectric functions change drastically with decreasing film thickness.[20] In the work of Naik *et al.*,[12] 5 nm thick layers were used. In another example, it

a)Author to whom correspondence should be addressed. Electronic mail: ruth.pachter@us.af.mil

was demonstrated that stoichiometric TiN(001) layers grown on MgO(001) are fully relaxed at the growth temperature, but changes are noted for sub-stoichiometric structures, where lattice constants decrease for TiN_x (x as low as 0.7) grown on Mg(001) at 700 °C,[23] which in turn will affect the optical properties.

At the same time, although density functional theory (DFT) calculations of structural and electronic properties of TiN bulk and surface structures were previously performed,[24–35] analysis of the optical properties at an *ab initio* level for this material was not addressed. The GW approximation within the framework of many-body perturbation theory[36,37] emerged as useful in prediction of optical properties using the BSE method to include excitonic effects.[38–40] GW-BSE (Bethe-Salpeter equation) is computationally intensive, but linear response time-dependent DFT (TDDFT) could be inadequate in predicting optical spectra of solid materials and depends on the exchange-correlation functional applied.[41] However, notwithstanding the experimental variations expected and the computational limitations, it is of interest in the first stage to obtain a reference frequency-dependent dielectric function theoretically by accurate first principles calculations for stoichiometric TiN.

In this work, we report calculations of the frequency-dependent real and imaginary parts of the dielectric function $(\varepsilon = \varepsilon^{(1)} + i\varepsilon^{(2)})$ for stoichiometric bulk TiN, as well as for surfaces that mimic the outermost layer, in comparison to SE data. The goal is to assess prediction of the complex refractive index in the low-energy region resulting from intraband transitions (lower than ca. 2 eV (Ref. 14)), and from interband transitions at higher energy. For this purpose, we performed a systematic study of structural, electronic, and optical properties for stoichiometric bulk TiN, and TiN(100), TiN(110), TiN(111) surfaces, applying DFT/TDDFT and GW methods. Dielectric functions were calculated using GW-BSE and TDDFT with generalized gradient approximation (GGA) and range-separated exchange-correlation functionals. We found that surface geometries and band structures were consistent with previous work. In benchmarking, the GW_0-BSE method was shown to be appropriate for the larger systems. In addition, comparison of the GW_0-BSE and TDDFT dielectric functions has shown that the functional is subject to validation with GW-BSE calculations. Analysis of the GW_0-BSE results in comparison to SE data demonstrated reasonable agreement with experiment, where variations due to experimental conditions have to be accounted for. This investigation will lead to further characterization of TiN thin films and provide a basis for the interpretation of measured optical properties.

II. METHODS

Calculations were performed using the Vienna *ab initio* simulation package VASP 5.3 (Refs. 42 and 43) within the framework of DFT. The projector augmented-wave (PAW) method was applied[43] for describing the electron-ion interaction, and the Perdew-Burke-Ernzerhof (PBE) GGA functional[44] was used, unless otherwise indicated. The Kohn-Sham equations[45,46] were solved using a plane-wave basis set, with an energy cutoff of 400 eV. For the surface calculations, a supercell with a vacuum region in the three-dimensional cell was used. Convergence for an adequate vacuum size was tested, and values of 10–16 Å were found to be large enough to ensure that the periodically repeated images do not interact. Atomic positions were relaxed until forces on each atom were smaller than 0.01 eV/Å. Monkhorst-Pack grid[47] sampling of the Brillouin zone (BZ) with $6 \times 6 \times 6$ k points for the bulk TiN and $6 \times 6 \times 1$ k points for surfaces was applied. A series of independent convergence tests that corroborate these parameters to provide the total energies within a few meV was performed. The cutoff energy was kept fixed when performing convergence testing of the number of k points, size of vacuum, number of surface layers, and relaxation algorithm used. Mixing and smearing parameters were chosen to obtain improved agreement with experiment.

TiN crystalizes in the NaCl lattice structure within the *Fm3m* space group. Three facets of the TiN surface were modeled, namely, TiN(100), TiN(110), and TiN(111), as well as bulk TiN. TiN(100) and TiN(110) surfaces were modeled by ten TiN layers with Ti and N atoms in the same plane (total of twenty atoms). Ti and N atoms in the TiN(111) surface are not in the same plane, but at a perpendicular distance of 1.22 Å from each other. This leads to two possibilities for the TiN(111) surface, namely, Ti- or N-terminated structures. Twenty one layers of TiN(111) with ten and eleven layers of either Ti- or N-termination were used. The (1×1) cell of surfaces is shown in Fig. 1. Optimization of TiN(100), TiN(110), and Ti- and N-terminated TiN(111) surfaces was carried out using PBE. The equilibrium lattice constant of bulk TiN, calculated by minimization of the total energy of the system with respect to the total volume of the unit cell, resulted in an optimized lattice constant of 4.25 Å, in agreement with the experimental values of 4.24 Å (Ref. 48) and 4.25 Å (Ref. 49) for bulk TiN, thus validating the functional used. Our result is also consistent with previous work using GGA, with values of 4.24–4.26 Å.[26,27,30–33] The lattice constant of bulk TiN calculated with LDA (local density approximation), of 4.175 Å, is underestimated compared to the GGA values.[26] Note that these values decrease for x smaller than 1 in TiN_x.[23]

Band structures were calculated by DFT and GW methods. Details on the implementation of the GW method within the PAW framework are given by Shishkin and Kresse in Refs. 50 and 51. GW-BSE[39] and TDDFT[52] were used for calculation of the frequency-dependent dielectric function. The large computational cost associated with GW calculations required the use of fewer surface layers, and the system size was reduced to 5 layers for the TiN(100), TiN(110) surfaces, and 11 layers for TiN(111) in this case. The iterative approach for GW calculations was carried out as follows. A non-self-consistent G_0W_0 evaluation of the quasiparticle self-energy was performed on top of the computationally less demanding DFT GGA calculation. Next, only G was iterated and W kept fixed (GW_0), generally shown to provide better agreement with experimental data,[51] and is relatively computationally less expensive. To perform self-consistent GW_0 (sc-GW_0) calculations, non-diagonal

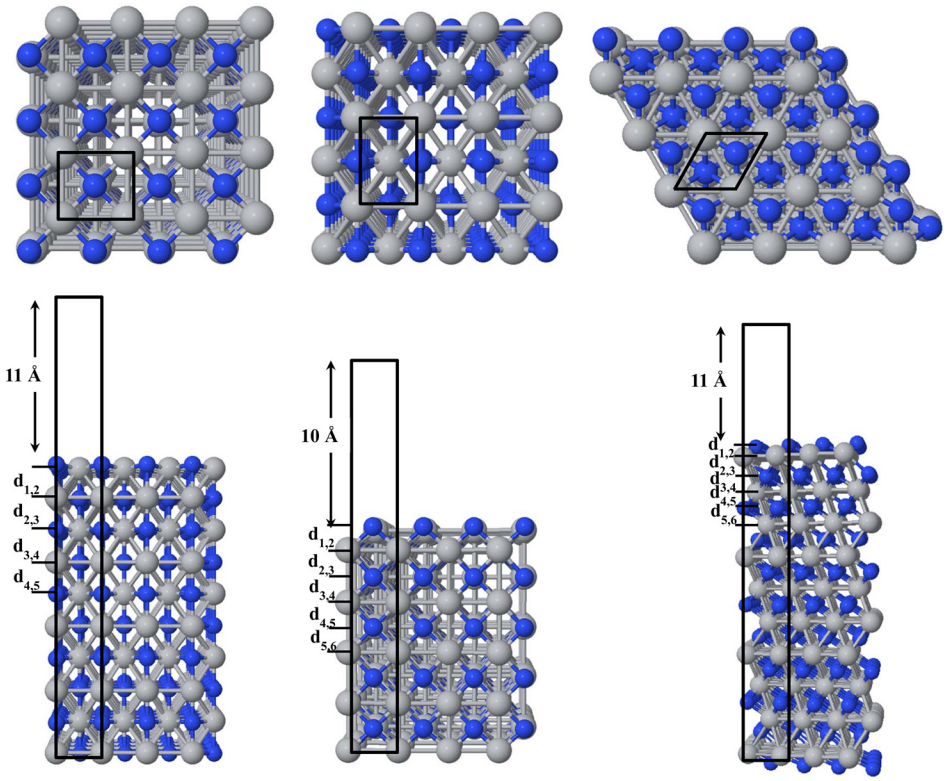

FIG. 1. Top and side views of TiN(100) (a), TiN(110) (b), and N-terminated TiN(111) (c) surfaces.

components of the self-energy are included in the orbital basis, only iterating G and keeping W fixed. sc-GW_0 is the most computationally intensive of the three approximations we applied, and the k-point mesh was reduced to $4 \times 4 \times 1$. GW calculations that fully update both Green's function G and the screened potential W, namely, full self-consistent GW (sc-GW), are computationally very intensive and their utility is still controversial,[41,51] while GW_0 or sc-GW_0 are commonly used.[53,54] Calculation of the dielectric function is carried out as a four step process. In the first step, a ground state DFT calculation is performed for occupied orbitals, and in the second stage, the wavefunction from the previous step is used to perform a ground state calculation with a large number of unoccupied empty bands and the dielectric matrix is calculated. In the third step, GW calculations (G_0W_0, GW_0, or sc-GW_0) are performed by using the wavefunction and dielectric matrix from the previous step, kept fixed throughout the various steps. At this stage, the band structure is also calculated. Band structures were calculated using both non-self-consistent and self-consistent evaluation of the quasiparticle self-energy. In the last step, the BSE is solved[39] to obtain the dielectric function.

TABLE I. ω_{pu} values (eV) for bulk TiN and TiN surfaces (eV).

ω_{pu}	GW_0-BSE	TDDFT/PBE	TDDFT/HSE
Bulk TiN	7.62	6.12	6.72
TiN(100)	4.76	3.60	3.97
TiN(110)	3.50	3.76	4.16
TiN(111)-Ti terminated	3.34	2.05	2.29
TiN(111)-N terminated	2.84	1.39	1.56

The imaginary part of the frequency-dependent dielectric function ($\varepsilon = \varepsilon^{(1)} + i\varepsilon^{(2)}$) in the PAW method (following the notation of Gajdoš *et al.*[55]) is given by the Cartesian tensor $\varepsilon^{(2)}_{\alpha\beta}(\omega) = \frac{4\pi^2 e^2}{\Omega} \lim_{q\to 0} \frac{1}{q^2} \sum_{c,v,\mathbf{k}} 2w_{\mathbf{k}} \delta(w_k \epsilon_{c\mathbf{k}} - \epsilon_{v\mathbf{k}} - w) \times \langle u_{c\mathbf{k}+e_\alpha q} | u_{v\mathbf{k}} \rangle \langle u_{c\mathbf{k}+e_{\alpha\beta} q} | u_{v\mathbf{k}} \rangle *$, where ω is in units of energy; Ω the volume of the primitive cell; $\boldsymbol{e}_\alpha$ unit vectors for the three Cartesian directions; the indices c and v refer to conduction and valence states, respectively; $u_{c\mathbf{k}}$ are the cell-periodic orbitals at $\mathbf{k}$. In the calculation of $\varepsilon^{(2)}_{\alpha\beta}(\omega)$, $\mathbf{k}$ is restricted to the irreducible wedge of the BZ. The real part of the dielectric tensor is obtained from the Kramers-Kroning transformation, given by $\varepsilon^{(1)}_{\alpha\beta}(\omega) = 1 + \frac{2}{\pi} P \int_0^\infty \frac{\varepsilon^{(2)}_{\alpha\beta}(\omega'')\omega'}{\omega'^2 - \omega^2 + i\eta} d\omega$, where P denotes the principal value of the integral and the small complex shift η (CSHIFT) is used for smoothing of the spectrum, which was set to 0.02 eV in all cases. Intraband

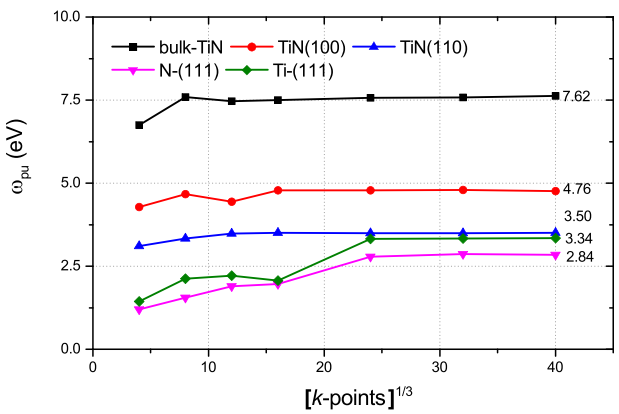

FIG. 2. Plasma frequency as a function of the number of k points for bulk TiN and TiN(100), TiN(110) and N- and Ti-terminated TiN(111) surfaces.

TABLE II. Percentage surface relaxation of TiN(100), TiN(110), and TiN(111) surfaces with respect to bulk-terminated distances (Å); T and D for TiN(100) and TiN(110) surfaces, as explained in the text. Negative and positive signs indicate contraction and expansion between the surfaces, respectively.

	TiN(100)		TiN(110)		TiN(111)	
	T	D	T	D	N-terminated	Ti-terminated
$d_{1,2}$	18.1	−1.10	15.02	−11.04	−36.63	−8.39
$d_{2,3}$	0.59	0.45	−8.76	4.70	25.92	0.28
$d_{3,4}$	−1.58	0.77	−2.88	0.17	−7.15	2.78
$d_{4,5}$	2.22	0.46	0.92	0.97	1.28	2.77
$d_{5,6}$		0.69	1.37	−0.89	1.57	−2.11
$d_{6,7}$					−0.41	0.39
$d_{7,8}$					0.23	0.85
$d_{8,9}$					0.82	−0.29
$d_{9,10}$					−1.41	1.07

transitions were calculated for the metallic system,[56,57] where the real part is expressed as $\varepsilon_{\alpha\beta}^{(1)intra}(\omega) = 1 - \frac{\bar{w}_{\alpha\beta}^2}{\omega^2}$, with the square of the intraband plasma frequency given by $\bar{w}_{\alpha\beta}^2 = \frac{4\pi e^2}{2}\sum_{n,\mathbf{k}} 2g_{\mathbf{k}} \frac{\partial f(\epsilon_{n\mathbf{k}})}{\partial \epsilon}\left(e_\alpha \frac{\partial \epsilon_{n\mathbf{k}})}{\partial \mathbf{k}}\right)\left(e_\beta \frac{\partial \epsilon_{n\mathbf{k}})}{\partial \mathbf{k}}\right)$. The frequency-dependent optical constants n and k were derived from the calculated dielectric function by $n = \sqrt{\frac{1}{2}(\varepsilon^{(1)} + \sqrt{\varepsilon^{(1)2} + \varepsilon^{(2)2}})}$ and $k = \sqrt{\frac{1}{2}(-\varepsilon^{(1)} + \sqrt{\varepsilon^{(1)2} + \varepsilon^{(2)2}})}$, as $n + ik = \sqrt{\varepsilon^{(1)} + i\varepsilon^{(2)}}$, and the electron energy loss spectrum (EELS) by $\varepsilon^{(2)}/(\varepsilon^{(1)2} + \varepsilon^{(2)2})$. The maximum frequency for the dense part of frequency grid (OMEGAMAX) was set to 100eV, and the number of frequency grid points (NEDOS) to a large value of 10000 for a dense set of data points. The number of bands (NBAND) was set to 64 for TiN bulk and surfaces, providing a significant number of empty bands. The band convergence was tested by increasing the number to 256, but no significant differences were noted; conventionally, the

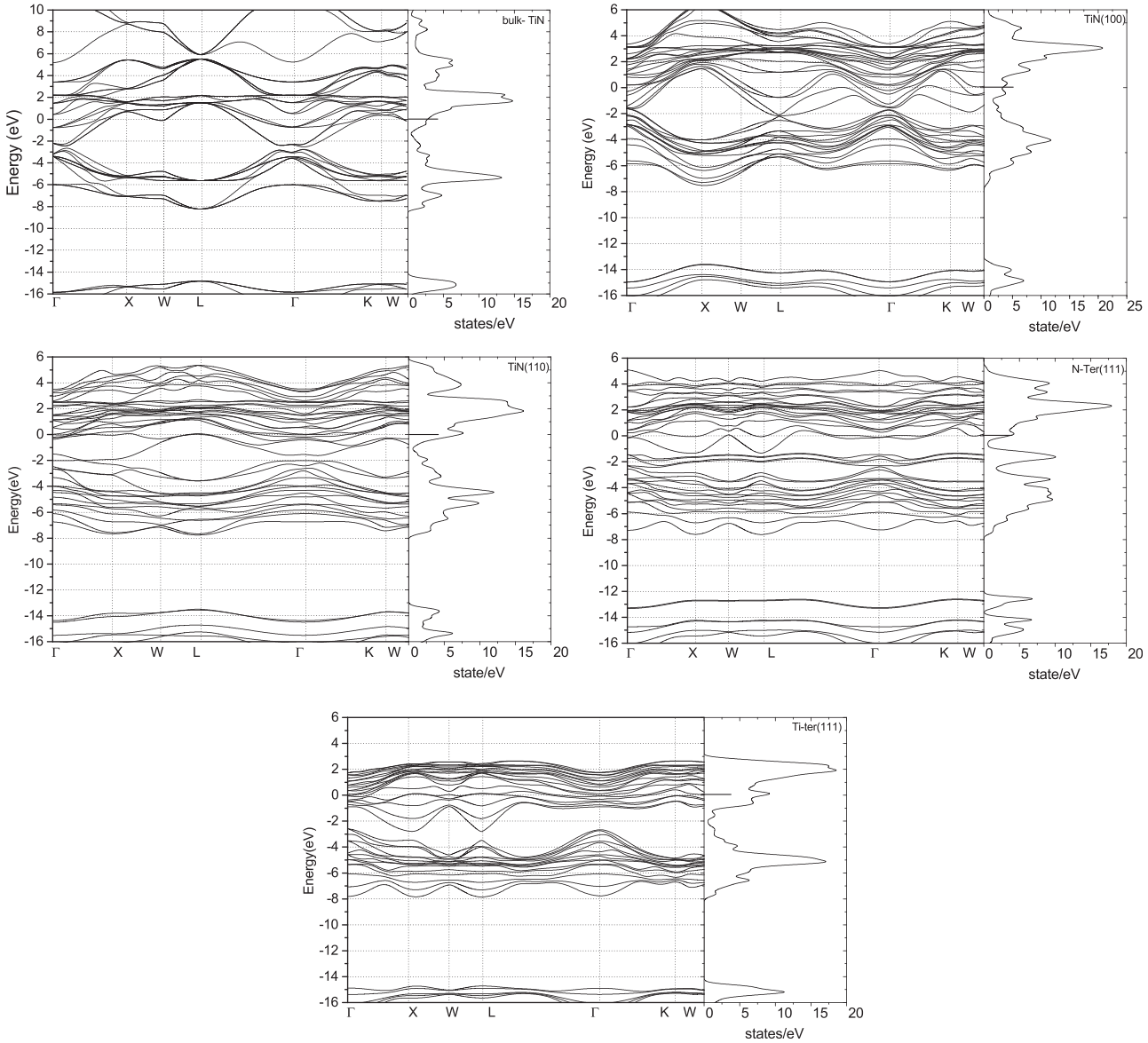

FIG. 3. Band structures and LDOS of bulk TiN and TiN(100), TiN(110), N- and Ti-terminated TiN(111) surfaces.

number of bands is set to half the number of electrons in the system, plus the total number of atoms, plus a few additional empty bands. Earlier studies suggested that reasonably converged results could be obtained by choosing bands that are 1.5 times the number of electrons.[58]

The *k*-point meshes were tested, specifically $4 \times 4 \times 4$, $5 \times 5 \times 5$, and $6 \times 6 \times 6$, and as small differences were noted, a $6 \times 6 \times 6$ *k*-point mesh for G_0W_0 and GW_0 and $4 \times 4 \times 4$ for sc-GW_0 calculations were selected. A larger mesh size greatly increases memory and computational requirements when solving the BSE and is not practical. Other studies using similar methods also found that such *k*-point meshes provide spectra in good agreement with the experimental data.[59] The number of empty bands and the size of the *k*-point mesh affect performance of the calculation by making it very demanding computationally, and our choice assured accurate prediction. We found that a very dense *k*-point mesh is essential to obtain a well-converged plasma frequency. Calculations of the plasma frequency with $4 \times 4 \times 4$ $(4 \times 4 \times 1)$ to $40 \times 40 \times 40$ $(40 \times 40 \times 1)$ *k*-point meshes for the bulk (surface) were performed. In most cases, we found the plasma frequency to reasonably converge around $24 \times 24 \times 24$ $(24 \times 24 \times 1)$ *k* points (see Table I and Fig. 2). However, such a dense mesh is not feasible for GW-BSE calculations because of the large memory requirements. Therefore, a sparser mesh was used to obtain the interband part of the dielectric function. For comparison, TDDFT calculations of the dielectric function using the PBE or the range-separated Heyd-Scuseria-Ernzerhof (HSE06, range-separation parameter 0.11 bohr^{-1} (Refs. 60 and 61)) functionals were performed. Ground state calculations were performed in this case using large *k*-point meshes of $12 \times 12 \times 12$ and $12 \times 12 \times 1$ for the bulk and surface systems, respectively, followed by TDDFT calculations.

III. RESULTS AND DISCUSSION

A. Surface morphology

TiN surfaces are known to undergo rippling, characterized by deviations in the interlayer separation from that of the bulk material, and by the distance between neighboring surface planes. In bulk-terminated surfaces prior to optimization, the perpendicular distance is zero, as the atoms lie in a plane. During structural relaxation, non-zero $d_{i,i+1}$ distances (T) and average displacement deviation of the planes (D) result. T and D values are summarized in Table II, reported as a percentage change, where positive and negative signs denote expansion or contraction between the surfaces, respectively. Bulk-terminated distances between two surface planes in TiN(100) and TiN(110) are 2.12 Å and 1.50 Å, respectively. As seen in Table II, surface formation for TiN(100) does not perturb the equilibrium distances significantly. Variation in T for the top layer compared to the bulk-terminated surface (18.1% or 0.18 Å) is consistent with the 17.9% change that was previously calculated.[26,32] Displacement T values are less than 2% for $d_{2,3}$ and $d_{3,4}$, lower than previously calculated, where a smaller number of layers was however used.[26,32] Surface relaxation quantified by D (see Table II) shows a small contraction of ca. −1%, while the rest of the TiN (100) surface layers expand slightly for compensation. Earlier calculations[26] reported a small contraction of about −2%, and an expansion of about 5%

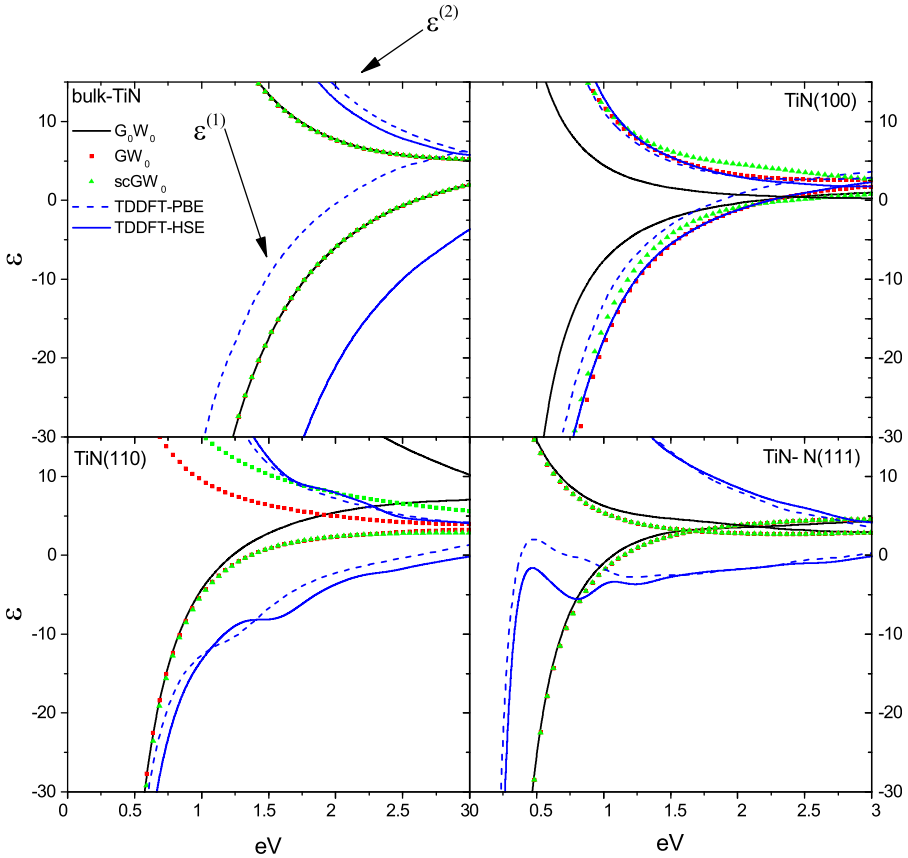

FIG. 4. Calculated dielectric functions ε as a function of the frequency (eV).

was also reported.[32] The rippling effect of the TiN(110) surface is similar to that of TiN(100), with T between the first and second layer of 0.15 Å (or 15%), decreasing for subsequent interlayer distances, comparable to previously calculated values of 0.146–0.163 Å.[26,31,32] A relatively large contraction in the distance between the first and second surface planes (D in Table II) was calculated, of −11%, resulting in an expansion of about 5% between the second and

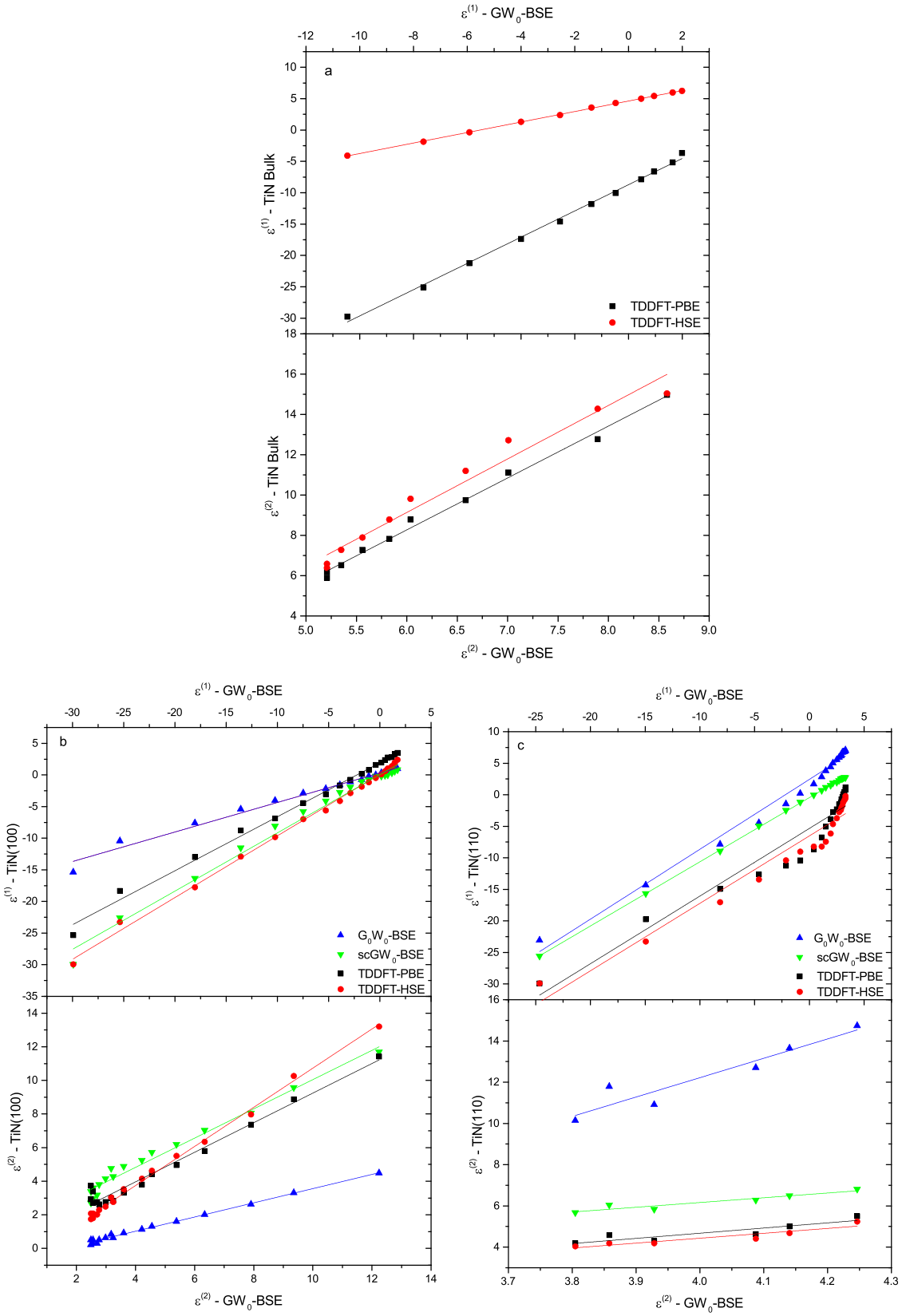

FIG. 5. Dielectric functions ε calculated at various levels of theory in comparison to GW_0-BSE for TiN bulk, TiN(100) and TiN(110) surfaces ((a)–(c)), respectively.

third layers, consistent with prior work.[26,31,32] Earlier calculations also showed that a converged value for the relaxation is found for a range of 9–11 atomic layers.[31]

The N-terminated TiN(111) surface demonstrated a large contraction between the first and second layers, accompanied by a smaller expansion for the second and third layers, while corresponding changes in the Ti-terminated TiN(111) surface were much smaller, as was similarly reported.[26,30,31] Note that the surface thickness in our material models ranges from ~1.4 nm for TiN(110) to ~2.5 nm

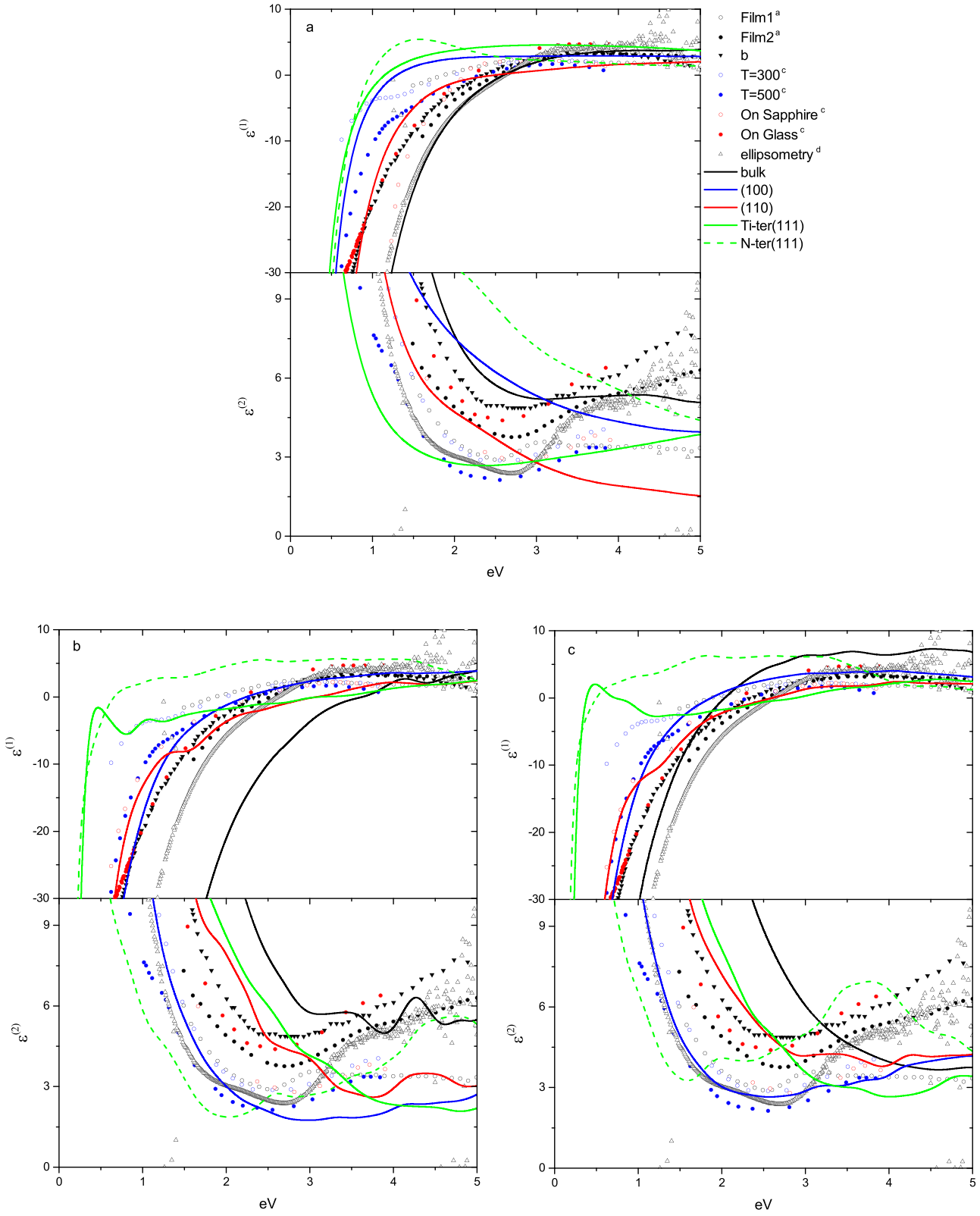

FIG. 6. Calculated dielectric functions for bulk TiN and TiN(100), TiN(110), and N- and Ti-terminated TiN(111) surfaces, as a function of frequency (eV), in comparison to SE data (a,[14] b,[20] c[8]) for (a) GW_0-BSE, (b) TDDFT-HSE, and (c) TDDFT-PBE.

for TiN(111). To understand effects of a larger number of layers on surface relaxation, molecular dynamics simulations with an appropriate force-field are required, for example, as performed by Sangiovanni *et al*. for admolecule transport on TiN(001) surfaces,[62] to be addressed in future work.

B. Electronic band structures

Using the optimized bulk and surface TiN structures, calculations of band structures were performed, as shown in Fig. 3. Our results are in agreement with the work of Yin *et al*.,[63] as shown Fig. S1 in the supplementary material.[64] Interband transitions for bulk TiN at ca. 1, 2.3, 3.0–3.9, and 5.0–6.2 eV were previously calculated,[14,16,28,65,66] and gaps in the 3.35–3.45 eV range were reported.[67–69] The local density of states (LDOS) of bulk TiN and the top layer of TiN(100), TiN(110), and TiN(111) surface facets are shown in Fig. 3. Three main regions can be identified. For bulk TiN, the lowest valence band comprises N *s* states and some hybridized Ti *d* states around −8 eV. The second lowest sub-band consists of strongly hybridized N *p* states and Ti *d* states representing the bonding part ranging from about −7 eV to the Fermi level (0 eV). The third region, the conduction band, consists mainly of Ti *d* states and a small degree of N *p* states corresponding to the antibonding part. When surfaces are formed, a change in the LDOS is noted. A small shift of the center of the band (∼0.5 eV) towards higher energies for the Ti atom in the top layer was calculated, which decreases when moving away from the surface. The shift is stronger for N atoms and amounts to 1 eV for TiN(100) and ca. 2 eV for TiN(111) surfaces. Strongest hybridization is noted for the N-terminated TiN(111) surface.

C. Optical properties

Frequency-dependent dielectric functions for bulk TiN, and TiN(100), TiN(110) and TiN(111) surfaces were calculated using the GW-BSE method and TDDFT with the PBE and HSE functionals. Comparison of the results is shown in Fig. 4 for bulk TiN and the considered surfaces. We compared GW_0-BSE results for up to 3 eV to those using other levels of theory because this is the spectral region that could be relevant to plasmonic applications. For analysis, calculated GW_0-BSE $\varepsilon^{(1)}$ and $\varepsilon^{(2)}$ (calculated at intervals of 0.125 eV), in comparison to G_0W_0-BSE, sc-GW_0-BSE and TDDFT, are shown in Figs. 5(a)–5(c) for TiN bulk and TiN(100) and TiN(110) surfaces, respectively (results for TiN(111) are shown in Fig. S2[64]). sc-GW_0-BSE dielectric functions are in good agreement with the GW_0-BSE results, but this is not always the case for G_0W_0-BSE. For example, for $\varepsilon^{(1)}$ for the TiN(100) surface, the slope in the linear regression is 0.5 in this case, but changes to 0.9–1 for other levels of theory (Fig. 5(b)). For bulk TiN, TDDFT using PBE and HSE functionals provided slopes that deviate considerably from 1, for example, 2.6–2.7 for $\varepsilon^{(2)}$ (Fig. 5(a)). GW_0-BSE $\varepsilon^{(1)}$ and $\varepsilon^{(2)}$ vs. TDDFT for TiN(110) demonstrate deviations, with correlation coefficients of 0.8–0.9, as compared to values close to 1 for bulk TiN and TiN(100). The agreement of TDDFT with GW_0-BSE for the TiN(111) surface is even worse (see Fig. S2), yet still to be considered because of the computational cost of GW-BSE calculations. Thus, calculated dielectric functions at the GW_0-BSE, and TDDFT-HSE and TDDFT-PBE levels were chosen for comparison with SE data.

Next, we compare GW_0-BSE dielectric functions for bulk TiN and TiN(100), TiN(110), and TiN(111) surfaces to experimental data, as summarized in Fig. 6(a), and values obtained using TDDFT with HSE and PBE functionals in Figs. 6(b) and 6(c), respectively. On comparing the experimental data for $\varepsilon^{(1)}$ in Ref. 8, measured at 300 °C, to the data in Ref. 14, and Ref. 20, a relative consistency is demonstrated, except for the region of up to about 2 eV, where intraband transitions are important, and where the plasma frequency is affected by deposition conditions. For $\varepsilon^{(2)}$, variations in the experimental data are larger, and so are differences in the theoretically determined values, and it is therefore difficult to compare with the calculated values directly. Plasma frequency ω_{pu} values are listed in Table I. Our results are consistent with previous calculations,[70] and with experimental measurements, however dependent on the bias voltage and temperature during synthesis. Larger voltage biases (from 40 V to 200 V) or temperatures (up to 600 °C) will increase ω_{pu} from ca. 5 eV up to 7.5 eV.[14] SE measured data are also dependent on the thickness,[14,20] and the stoichiometry of the thin film with nitrogen vacancies or atom incorporation in interstitial positions.[71] TDDFT results reproduce less well experimental data, particularly for the N-terminated TiN(111) surface. Notably, for both the $\varepsilon^{(1)}$ and $\varepsilon^{(2)}$, the N-terminated TiN(111) surface provided poorer

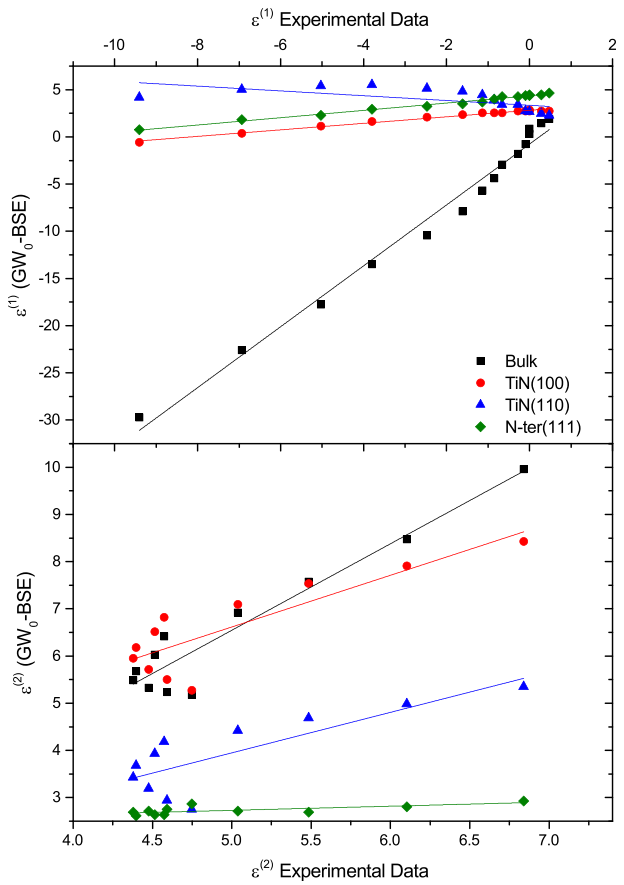

FIG. 7. Calculated dielectric functions ε vs. experimental data from Ref. 8.

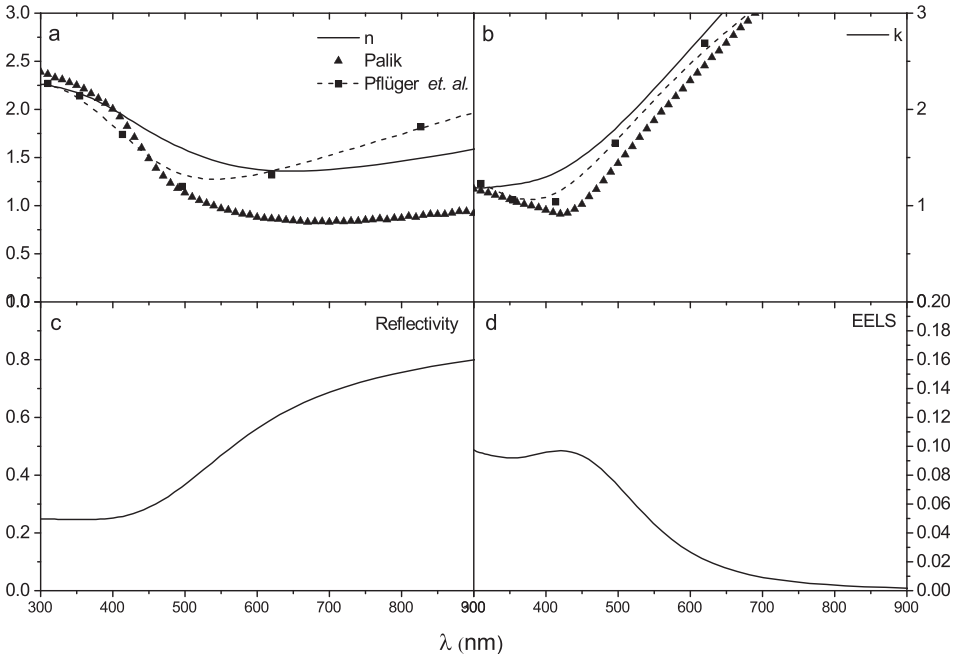

FIG. 8. Refractive index n (a), extinction coefficient k (b), reflectivity (c), and EELS spectrum (d) for bulk TiN at the sc-GW_0-BSE level of theory.

general agreement with experiment. As we noted in examining the surface structure, the N-terminated TiN(111) surface demonstrated a large contraction between the first and second layers, and further investigation of details of structural parameter changes of the surface is to be undertaken in future work.

For a quantitative comparison with GW_0-BSE, we used the data in Ref. 8, as shown in Fig. 7. A reasonable agreement with experiment is demonstrated for bulk TiN for $\varepsilon^{(1)}$ and $\varepsilon^{(2)}$ (correlation coefficients of 0.9–1). However, this is generally not the case for TiN surfaces as expected, because the SE data we compared to has been obtained for larger thicknesses than the outermost layers modeled. Validation of the theoretical results depends on careful experimental characterization of the structure, and calculations for amorphous structures will be carried out in future work. Optical constants, namely, refractive index n and extinction coefficient k for bulk TiN calculated at the sc-GW_0-BSE level, are shown in Figs. 8(a) and 8(b), respectively. The theoretical results overestimate the data from Palik,[72] commonly used in electromagnetic simulations of plasmonic nanostructures, particularly in the low-energy spectral region, as expected. A better agreement is noted with the data of Pflüger *et al.*[49] The reflectivity spectrum of bulk TiN is shown Fig. 8(c), having a high absolute value at low energies, indicative of its metallic behavior, and consistent with SE measurements.[16] The EELS spectrum in Fig. 8(d) is also consistent with experiment for bulk TiN.[16]

IV. CONCLUSION

In this work, we have undertaken an investigation of electronic and optical properties of stoichiometric bulk TiN, and TiN(100), TiN(110), TiN(111) surfaces, benchmarking the band structure and comparing the dielectric function to SE data obtained for realistic samples. To address theoretical challenges in prediction of electronic and optical properties of solid materials, both DFT and many-body GW methods were applied, ranging from G_0W_0 to partially self-consistent sc-GW_0, and TDDFT (using the PBE and HSE functionals) and GW-BSE for dielectric function predictions. The structural ripple effect in TiN was quantified by optimization of surface structures, and the optimized structures used for calculation of the electronic and optical properties. The band structure we calculated demonstrated consistency with previous work for bulk TiN. GW_0-BSE dielectric functions, analyzed in comparison to SE data of the real $\varepsilon^{(1)}$ and imaginary $\varepsilon^{(2)}$ parts of the dielectric function, demonstrated qualitative agreement with experiment, where variations due to experimental sample characteristics have to be considered. Consistency with experiment was also shown in calculation of the plasma frequency, as well as the reflectivity and EELS spectra. We found that TDDFT is less suitable for evaluation of the optical constants n and k, yet could be considered upon benchmarking with higher level calculations. A calculated dielectric function for materials for which experimental characterization is complicated can be used in electromagnetic simulations of plasmonic nanostructures to assess bounds of performance, or in design of multi-layer optical coatings that require knowledge of the frequency-dependent complex refractive index.

ACKNOWLEDGMENTS

We acknowledge fruitful discussion with Chintalapalle Ramana, University of Texas at El Paso, Brandon Howe, AFRL, and Antonio Mei, University of Illinois. We gratefully acknowledge the computer resources and helpful assistance provided by the AFRL DSRC for High Performance Computing.

[1]L. Toth, *Transition Metal Carbides and Nitrides, Refractory Materials Series* (Academic Press, New York/London, 1971), p. 91.
[2]H. O. Pierson, *Handbook of Refractory Carbides & Nitrides: Properties, Characteristics, Processing and Apps* (William Andrew, 1996).

[3]L. I. Johansson, Surf. Sci. Rep. **21**, 177 (1995).
[4]F. Vaz, P. Machado, L. Rebouta, P. Cerqueira, P. Goudeau, J. P. Riviere, E. Alves, K. Pischow, and J. de Rijk, Surf. Coat. Technol. **174–175**, 375 (2003).
[5]P. H. Mayrhofer, C. Mitterer, L. Hultman, and H. Clemens, Prog. Mater. Sci. **51**, 1032 (2006).
[6]L. Wu, H. Y. Yu, X. Li, K. L. Pey, J. S. Pan, J. W. Chai, Y. S. Chiu, C. T. Lin, J. H. Xu, H. J. Wann, X. F. Yu, D. Y. Lee, K. Y. Hsu, and H. J. Tao, Appl. Phys. Lett. **96**, 113510 (2010).
[7]A. E. Khalifa and M. A. Swillam, Proc. SPIE **8981**, 89811R (2014).
[8]G. V. Naik, J. L. Schroeder, X. J. Ni, A. V. Kildishev, T. D. Sands, and A. Boltasseva, Opt. Mater. Express **2**, 478 (2012).
[9]U. Guler, G. V. Naik, A. Boltasseva, V. M. Shalaev, and A. V. Kildishev, Appl. Phys. B-Lasers Opt. **107**, 285 (2012).
[10]G. V. Naik, V. M. Shalaev, and A. Boltasseva, Adv. Mater. (Weinheim, Ger.) **25**, 3258 (2013).
[11]U. Guler, J. C. Ndukaife, G. V. Naik, A. G. A. Nnanna, A. V. Kildishev, V. M. Shalaev, and A. Boltasseva, Nano Lett. **13**, 6078 (2013).
[12]G. V. Naik, B. Saha, J. Liu, S. M. Saber, E. A. Stach, J. M. K. Irudayaraj, T. D. Sands, V. M. Shalaev, and A. Boltasseva, Proc. Natl. Acad. Sci. U. S. A. **111**, 7546 (2014).
[13]K. Yee, IEEE Trans. Antennas Propag. **14**, 302 (1966).
[14]P. Patsalas and S. Logothetidis, J. Appl. Phys. **90**, 4725 (2001).
[15]P. Patsalas and S. Logothetidis, J. Appl. Phys. **93**, 989 (2003).
[16]M. Benhamida, A. Meddour, S. Zerkout, and S. Achour, J. Mol. Struct.: THEOCHEM **777**, 41 (2006).
[17]S. Wrehde, M. Quaas, R. Bogdanowicz, H. Steffen, H. Wulff, and R. Hippler, Vacuum **82**, 1115 (2008).
[18]G. Duan, G. Zhao, L. Wu, X. Lin, and G. Han, Appl. Surf. Sci. **257**, 2428 (2011).
[19]K. Vasu, M. G. Krishna, and K. A. Padmanabhan, Appl. Surf. Sci. **257**, 3069 (2011).
[20]H. Van Bui, A. Y. Kovalgin, and R. A. M. Wolters, Appl. Surf. Sci. **269**, 45 (2013).
[21]L. E. Koutsokeras, G. M. Matenoglou, and P. Patsalas, Thin Solid Films **528**, 49 (2013).
[22]N. White, A. L. Campbell, J. T. Grant, R. Pachter, K. Eyink, R. Jakubiak, G. Martinez, and C. V. Ramana, Appl. Surf. Sci. **292**, 74 (2014).
[23]C. S. Shin, S. Rudenja, D. Gall, N. Hellgren, T. Y. Lee, I. Petrov, and J. E. Greene, J. Appl. Phys. **95**, 356 (2004).
[24]P. Blaha and K. Schwarz, Int. J. Quantum Chem. **23**, 1535 (1983).
[25]R. Ahuja, O. Eriksson, J. M. Wills, and B. Johansson, Phys. Rev. B **53**, 3072 (1996).
[26]M. Marlo and V. Milman, Phys. Rev. B: Condens. Matter Mater. Phys. **62**, 2899 (2000).
[27]M. Siodmiak, N. Govind, J. Andzelm, N. Tanpipat, G. Frenking, and A. Korkin, Phys. Status Solidi B **226**, 29 (2001).
[28]Z. Dridi, B. Bouhafs, P. Ruterana, and H. Aourag, J. Phys.: Condens. Matter **14**, 10237 (2002).
[29]N. Cruz Hernandez, J. Graciani, and J. F. Sanz, Surf. Sci. **541**, 217 (2003).
[30]S. Hao, B. Delley, and C. Stampfl, Phys. Rev. B **74**, 035402 (2006).
[31]C. Wang, Y. Dai, H. Gao, X. Ruan, J. Wang, and B. Sun, Solid State Commun. **150**, 1370 (2010).
[32]S. Sanyal, U. V. Waghmare, and J. A. Ruud, Appl. Surf. Sci. **257**, 6462 (2011).
[33]T. Lee, B. Delley, C. Stampfl, and A. Soon, Nanoscale **4**, 5183 (2012).
[34]R.-Q. Zhang, T.-H. Lee, B.-D. Yu, C. Stampfl, and A. Soon, Phys. Chem. Chem. Phys. **14**, 16552 (2012).
[35]L. Xiao, Y. Su, H. Chen, S. Liu, M. Jiang, P. Peng, and S. Liu, Appl. Phys. Lett. **99**, 061906 (2011).
[36]L. Hedin, Phys. Rev. **139**, A796 (1965).
[37]M. S. Hybertsen and S. G. Louie, Phys. Rev. B: Condens. Matter **34**, 5390 (1986).
[38]E. Salpeter and H. A. Bethe, Phys. Rev. **84**, 1232 (1951).
[39]S. Albrecht, L. Reining, R. Del Sole, and G. Onida, Phys. Rev. Lett. **80**, 4510 (1998).
[40]M. Rohlfing and S. G. Louie, Phys. Rev. B: Condens. Matter Mater. Phys. **62**, 4927 (2000).
[41]Y. Ping, D. Rocca, and G. Galli, Chem. Soc. Rev. **42**, 2437 (2013).
[42]G. Kresse and J. Furthmuller, Comput. Mater. Sci. **6**, 15 (1996).
[43]G. Kresse and D. Joubert, Phys. Rev. B **59**, 1758 (1999).
[44]J. P. Perdew, K. Burke, and M. Ernzerhof, Phys. Rev. Lett. **77**, 3865 (1996).
[45]P. Hohenberg and W. Kohn, Phys. Rev. **136**, B864 (1964).
[46]W. Kohn and L. J. Sham, Phys. Rev. **140**, A1133 (1965).
[47]H. J. Monkhorst and J. D. Pack, Phys. Rev. B **13**, 5188 (1976).
[48]N. Schönberg, Acta Chem. Scand. **8**, 213 (1954).
[49]J. Pflüger, J. Fink, W. Weber, K. P. Bohnen, and G. Crecelius, Phys. Rev. B **30**, 1155 (1984).
[50]M. Shishkin and G. Kresse, Phys. Rev. B: Condens. Matter Mater. Phys. **74**, 035101/1 (2006).
[51]M. Shishkin and G. Kresse, Phys. Rev. B **75**, 235102 (2007).
[52]J. Paier, M. Marsman, K. Hummer, G. Kresse, I. C. Gerber, and J. G. Ángyán, J. Chem. Phys. **124**, 154709 (2006).
[53]G. Onida, L. Reining, and A. Rubio, Rev. Mod. Phys. **74**, 601 (2002).
[54]J. Deslippe and S. G. Louie, *Ab Initio Theories of the Structural, Electronic, and Optical Properties of Semiconductors: Bulk Crystals to Nanostructures* (Elsevier B.V., 2011), Vol. 1.
[55]M. Gajdos, K. Hummer, G. Kresse, J. Furthmuller, and F. Bechstedt, Phys. Rev. B: Condens. Matter Mater. Phys. **73**, 045112/1 (2006).
[56]J. Harl, G. Kresse, L. D. Sun, M. Hohage, and P. Zeppenfeld, Phys. Rev. B: Condens. Matter Mater. Phys. **76**, 035436/1 (2007).
[57]J. Harl, Ph.D. thesis, Uni Wien, 2008.
[58]J. Harl and G. Kresse, Phys. Rev. Lett. **103**, 056401 (2009).
[59]Y. Ping, D. Rocca, and G. Galli, Phys. Rev. B: Condens. Matter Mater. Phys. **87**, 165203/1 (2013).
[60]J. Heyd, G. E. Scuseria, and M. Ernzerhof, J. Chem. Phys. **118**, 8207 (2003).
[61]A. V. Krukau, O. A. Vydrov, A. F. Izmaylov, and G. E. Scuseria, J. Chem. Phys. **125**, 224106/1 (2006).
[62]D. G. Sangiovanni, D. Edstroem, L. Hultman, V. Chirita, I. Petrov, and J. E. Greene, Phys. Rev. B **86**, 155443 (2012).
[63]D. Yin, X. Peng, Y. Qin, and Z. Wang, J. Appl. Phys. **108**, 033714 (2010).
[64]See supplementary material at http://dx.doi.org/10.1063/1.4935813 for band structure of bulk TiN and calculated dielectric function for TiN(111).
[65]V. Ern and A. C. Switendick, Phys. Rev. **137**, A1927 (1965).
[66]A. Schlegel, P. Wachter, J. J. Nickl, and H. Lingg, J. Phys. C **10**, 4889 (1977).
[67]M. N. Solovan, V. V. Brus, E. V. Maistruk, and P. D. Maryanchuk, Inorg. Mater. **50**, 40 (2014).
[68]Y. Massiani, A. Medjahed, and G. Picq, Thin Solid Films **207**, 109 (1992).
[69]D. W. Fischer and W. L. Baun, J. Appl. Phys. **39**, 4757 (1968).
[70]J. Kim, S.-H. Jhi, and L. K. Ryeol, J. Appl. Phys. **110**, 083501 (2011).
[71]E. Penilla, F. G. Perez-Gutierrez, W. Duvall, G. Aguilar, and J. Wang, Thin Solid Films **524**, 272 (2012).
[72]E. D. Palik, *Handbook of Optical Constants of Solids* (Academic Press, 1998), Vol. 3.